Co-published by
Institute of Fluid-Flow Machinery
Polish Academy of Sciences
Committee on Thermodynamics and Combustion
Polish Academy of Sciences

http://www.imp.gda.pl/archives-of-thermodynamics/

Theoretical investigation for optimal thermal and thermodynamic performance of flat-plate solar collector with nanofluids

Vikash Kumar Gorai[a], Mukesh Kumar[a], Rahul Singh[b], Mukesh Kumar Sahu[c*]

[a]Cambridge Institute of Technology, Tatisilwai, Ranchi, Jharkhand, 835103, India
[b]Amity University, Ranchi, Jharkhand, 834001, India
[c]Kalinga University, Kotni, Naya Raipur, Chhattisgarh, 492101, India
*Corresponding author email: mukeshkumar.sahu@kalingauniversity.ac.in

Received: 22.04.2024; revised: 05.11.2024; accepted: 06.12.2024

Abstract

In this work, an analytical study is carried out on the performance of copper-based nanoparticles and water in flat-plate solar collectors. The effect of copper-based nanoparticles on various thermophysical properties of collectors has been studied and compared with water under the same conditions. The effects of temperature rise parameter from 0.0018 to 0.025, volume percentage of nanoparticles from 0 to 1 and mass flow rate in the range of 0.012 to 0.170 kg/s have been considered. The mass flow rate range covers both laminar and turbulent flow conditions. A detailed parametric study was carried out by developing appropriate MATLAB codes for various performance and energy equations to investigate the effects of volume percentage of nanoparticles and mass flow rate on the basic thermophysical properties and performance parameters, including Nusselt number, heat transfer coefficient, collector plate factor, heat removal factor, Reynolds number, collector heat gain, fluid outlet temperature and thermal efficiency. A new number has been introduced to find out the optimal value of mass flow rate for optimizing collector performance. From the analysis it was found that water collector achieved the maximum thermal efficiency of 53.7% for the highest value of mass flow rate of 0.1675 kg/s. For the nanofluid collector, the maximum efficiency is 70.5% for a nanofluid volume fraction of 0.48 and for the highest considered value of mass flow rate of 0.1675 kg/s. The nanofluid collector is predicted to provide up to 16.8% higher energy efficiency than the water collector.

Keywords: Nanofluid; Flat-plate solar collector; Density; Efficiency

Vol. 46(2025), No. 1, 155–167; doi: 10.24425/ather.2025.154189

Cite this manuscript as: Gorai, V.K., Kumar, M., Singh, R., & Sahu, M.K. (2025). Theoretical investigation for optimal thermal and thermodynamic performance of flat-plate solar collector with nanofluids. *Archives of Thermodynamics*, 46(1), 155–167.

1. Introduction

The use of different types of non-conventional renewable energy sources is necessary to fulfill the continuously increasing energy demands. In order to use and convert solar energy into useful thermal energy for the various mankind applications, it is essential that solar thermal energy conversion systems deliver maximum efficiencies [1]. To improve the performance of thermal systems nanofluids are also widely used for the heat transfer, cooling and others applications [2]. The use of nanofluids and nanotechnology in thermal energy conversion systems improves its performance without any harmful environmental impact.

Nanofluid is a colloidal mixture of nano-sized particles in a host (base) fluid to affect the thermophysical properties and improve the heat transfer characteristics of base fluids, which are useful for different practical applications [3]. Nanofluids are now used frequently as coolants, lubricants, hydraulic fluids and metal cutting fluids. There are many research works that concentrate on nanofluids containing different nanoparticles with various volume concentrations and sizes [4]. Various base

Nomenclature

A_c – collector surface area, m^2
C_b – bond conductance, W/(m^2 K)
C_P – specific heat capacity, J/(kg K)
D – diameter of tube, m
D_i – inner diameter of tube, m
f – friction factor
F – fin efficiency
F' – collector efficiency factor
F_P – collector efficiency factor
F_R – heat removal factor
h – heat transfer coefficient, W/(m^2 K)
I – intensity of solar radiation, W/m^2
k – thermal conductivity, W/(m K)
L – length of collector, m
Nu – Nusselt number
m – mass flow rate, kg/s
Pr – Prandtl number
Qu – useful heat gain, W
Re – Reynolds number
t – thickness, m
T – temperature, K
T_{fm} – mean fluid temperature, K
T_{pm} – mean plate temperature, K
TEIF– thermal efficiency improvement factor
ΔT – temperature drop, = $T_{fo} - T_{fi}$, °C
$\Delta T/I$ – temperature rise parameter, °C m^2/W
U_L – overall heat loss coefficient, W/(m^2 K)
V – velocity of fluid in the collector, m/s
W – riser tube spacing, m

Greek symbols

η_{th} – thermal efficiency
μ – dynamic viscosity, N s/m^2
ρ – density, kg/m^3
ϕ – volume fraction
$(\tau\alpha)$ – effective transmittance-absorptance product

Subscripts and Superscripts

a – ambient
avg – average
bf – base fluid
f – fluid
in – inlet
ir – inner
out – outlet
nf – nanofluid
np – nanoparticle
p – plate

fluids such as ethylene glycol, form amide, water, etc., have been used by the researchers. The enhancement in thermal properties is achieved by mixing nano-sized particles, dispersed uniformly in the base fluids [5]. Nanoparticles have a larger relative surface area since particle size is very small, thus providing higher suspension stability that improves the thermal conductivity of the mixture [6,7].

Nanofluid is a colloidal suspension of nanoparticles of size 1 to 100 nm (10^{-9} m) in the base fluid, and this is the term first given by Choi in 1995 [8]. Depending on the application, nanofluids have been made of various materials such as metals, metal oxides, ceramics and carbon nanotubes (CNT). Alim et al. [9] carried out a theoretical study, investigating the effects of 4 different nanoparticles (NPs), namely alumina oxide (Al_2O_3), titanium oxide (TiO_2), silicon dioxide (SiO_2), and copper oxide (CuO), on thermal energy efficiency and entropy generation (EG), based on the second law of thermodynamics for the flat-plate collectors. They explored the effects of different concentrations and volume flow rates on the efficiencies of the flat-plate collector and found that CuO nanoparticles deliver the highest enhancement over the other types of nanoparticles.

Moghadam et al. [10] carried out experimental research using the CuO nanoparticles and water as base fluid in the flat-plate collector. They found an enhancement in the collector efficiency with increasing the mass flow rate for both types of flat-plate collectors, i.e. for nanofluid based and water based flat plate collectors.. Shojaeizadeh et al. [11] carried out a theoretical study for the exergy performance considering Al_2O_3–H_2O nanofluid as the heat transfer fluid (HTF) in a flat-plate collector. They investigated various parameters, including volume concentration, solar radiation, plate absorber area, mass flow rate, ambient temperature, and the fluid inlet temperature, on the flat-plate collector exergy efficiency.

Mahian et al. [12] carried out a theoretical study considering Al_2O_3 nanofluid in a flat-plate solar collector. They have investigated the effects of solar radiation and ambient temperature on the entropy generation in the collector. They took the nanoparticles with different sizes as 25, 50, 75 and 100 nm, volume percentages of up to 4 vol% and mass flow rates within the range between 0.1 and 0.8 kg/s. They reported that, as the nanofluid concentration enhances, the entropy generation rate decreases.

Said et al. [13] performed theoretical analysis for a flat-plate collector using single wall carbon nanotubes (SWCNTs) based nanofluid. They evaluated and compared the 2nd law exergetic efficiency and pumping power performance of the SWCNT nanofluid based solar collector with the Al_2O_3, SiO_2 and TiO_2 nanofluid based solar collectors. Sint et al. [14] carried out theoretical analysis using the program developed in MATLAB software in order to estimate the thermal performance of the flat-plate solar collector by using CuO and H_2O based nanofluid. They reported that the collector efficiency is a function of volume percentage and nanoparticle size. The collector efficiency was found to be maximum when the values of the total heat loss coefficient are at a minimum. Furthermore, the collector efficiency was found to be maximum when the collector heat removal factor have its maximum value.

Tong et al. [15] carried out experimental research using H_2O, Al_2O_3 with base fluid H_2O, and CuO with base fluid H_2O. They have evaluated the absorber performance for a fixed flow rate of 0.047 kg/s. They have reported that Al_2O_3 in a H_2O base fluid at a volume percentage of 0.01%, has the highest energy efficiency of 77.5% while CuO with H_2O base fluid has maximum efficiency of 73.9%. They also found that entropy generation was

the highest for H_2O based collector and the lowest for Al_2O_3 nanofluid with 1.0 %vol. fraction.

Esen et al. [16] reported the modelling of new solar air heater (SAH) efficiency by using the least-squares support vector machine (LS-SVM) method. They carried out their research for the SAH with double-pass channel. They have compared the predicted and experimental results and after that proposed that LS-SVM model can be used for estimating the efficiency of SAHs with reasonable accuracy. In another work, Esen et al. [17] carried out their study on SAH system by using artificial neural network (ANN) and wavelet neural network (WNN) models. The authors compared the predicted and experimental results and proposed that WNN model can be used for estimating some parameters of SAHs with sufficient accuracy.

Ozgen et al. [18] performed an experimental investigation using aluminium cans as an absorbing plate in the double-pass channel of a flat-plate SAH. They considered different arrangements of the aluminium cans in the absorber plate. For the first type (Type I) they were staggered as zigzag and for the second one (Type II) they were arranged in order. Type III was a flat absorber plate (without cans). They used two values of air mass flow rates, 0.03 kg/s and 0.05 kg/s. They obtained the highest thermal efficiency for the Type I configuration at a mass flow rate of 0.05 kg/s.

In the study of Esen et al. [19], experiments were performed to find out how the use of different refrigerants affects thermal performance of a two-phase thermosyphon solar collector. Three identical small-scale solar water heating systems, using refrigerants R-134a, R407C, and R410A, were constructed and tested side-by-side under various environmental and load conditions. Oflaz et al. [20] carried out experimental study to explore the thermohydraulic performance of a heat exchanger tube with the combined use of SiO2-water nanofluids with newly designed conical wire inserts. The inserts were placed in a tube with five distances ranging from 0 to 33.6 mm and SiO_2-water nanofluids were used at four volume concentrations (0.5–1.25%). They obtained the best performance evaluation criteria of 1.75 at Reynolds number of 3338 and volume concentration of 1.25% for conical wire inserts with pitch ratio of 0.

Based on the literature review it is found that most of the studies have been carried out using alumina oxide (Al_2O_3) nanoparticles. To the best knowledge of the authors, the effects of copper (Cu) nanofluid as water-based fluid on the flat plate solar collector characteristics and the comparison with a water-based collector for both, i.e. laminar and turbulent flow conditions have not been studied in detail by any investigator up to now. The effect of temperature rise parameter and nanofluid volume fraction in the range of 0–1 have also not been reported by the researchers. Thermophysical properties, and various energy and performance parameters for the collectors have been evaluated by developing suitable MATLAB code.

2. Solar collector system description and methodology

In the flat collectors, nanofluid and water enters through circular shape riser tubes (Fig. 1). For the present analysis a single transparent glass cover has been considered. To minimize the losses proper insulation is provided in the bottom and on the sides of the collectors.

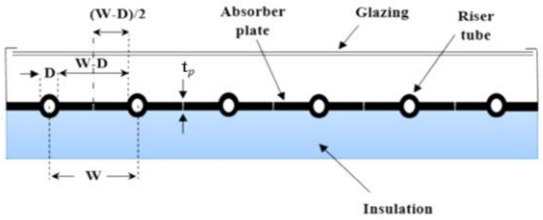

Fig. 1. A schematic of the structure and basic components of a flat-plate solar collector.

The input data for the performance evaluation of the collector, including the physical dimensions of the flat-plate collector, its operating parameters like mass flow rate and inlet temperature, as well as environmental conditions like the solar irradiance, wind velocity, and ambient temperature, were considered as given in Table 1. The arrangement of the flat-plate collector and riser tubes that were considered in the present analysis is shown in detail in Fig. 1.

Table 1. Specifications of the collector and parameters for the present analysis.

Parameter		Value	Unit
Collector dimension	length	2.0	m
	width	0.95	
	height	0.095	
Absorption area, A_c		1.90	m^2
Header pipe diameter, D_H		0.022	m
Distance between two parallel tubes, W		0.145	m
Riser pipe diameter, D_o		0.01	m
Riser pipe thickness, t		0.9×10^{-3}	m
Collector tubes diameter, D		0.009	m
Working fluid		Cu nanofluid and water (H_2O) as the base fluid	
No. of glazing, Ng		1	
Thermal emission of absorption sheet, εp		0.07	
Solar absorption of absorption sheet		0.95	
Glass cover emissivity, εg		0.88	
Collector plate thickness, t		0.005	m
Collector plate thermal conductivity, k_p		383	W/(m K)
Collector tilt		35	deg
Insulation thermal conductivity, k_i		0.05	W/(m K)
Back insulation thickness, t_b		0.05	m
Solar radiation, I		900	W/m^2
Wind velocity, V_w		3.2	m/s
Ambient temperature, T_a		300	K
Inlet temperature, T_i		301	K
Mass flow rate, m		0.012–0.170	kg/s

2.1. Properties of nanofluids

2.1.1. The density of the nanofluid, is evaluated based on the principle of the mixture rule as follows [20−22]:

$$\rho_{nf} = \phi\rho_{np} + (1-\phi)\rho_{bf}, \quad (1)$$

where ϕ represents volume fraction of nanoparticles, and subscripts *np* and *bf* stand for nanoparticles and base fluid, respectively.

2.1.2. The specific heat of a nanofluid is predicted by using the thermal equilibrium model:

$$C_{P,nf} = \frac{\phi(\rho C)_{np}+(1-\phi)(\rho C)_{bf}}{\rho_{nf}}. \quad (2)$$

2.1.3. The thermal conductivity of nanofluid can be evaluated as the equation given by Maxwell, which shows a good agreement with the experimental data over the other proposed models [9,10]:

$$\frac{k_{nf}}{k_{bf}} = \frac{k_{np}+2k_{bf}-2\phi(k_{bf}-k_p)}{k_{np}+2k_{bf}+\phi(k_{bf}-k_p)}. \quad (3)$$

The conductivity of the base fluid is evaluated at the average temperature (T_{avg}) from the following equation [14]:

$$k_{bf} = 0.6065\left[1.488445 + 4.12292\left(\frac{T_{avg}}{298.15}\right) - 1.63866\left(\frac{T_{avg}}{298.15}\right)\right]. \quad (4)$$

2.1.4. Dynamic viscosity of a nanofluid can be calculated by the equation that follows from the Brinkman's model

$$\frac{\mu_{nf}}{\mu_{bf}} = \frac{1}{(1-\phi)^{2.5}}, \quad (5)$$

where the viscosity of the base fluid is given as

$$\mu_{bf} = 2.414\times10^{-5}\times 10^{\frac{247.8}{Tavg-140}}. \quad (6)$$

2.1.5. The energy efficiency of the solar collector is defined by [23]

$$\eta_{th} = \frac{Qu}{A_c I}, \quad (7)$$

where A_c is a collector surface area, I is the intensity of solar radiation, and Qu represents the useful heat gain from available solar energy and is expressed by [23]

$$Qu = mC_P(T_{out} - T_{in}). \quad (8)$$

2.1.6. Useful heat gain can also be calculated as

$$Qu = A_c F_R[I(\tau\alpha) - U_L(T_{fm} - T_a), \quad (9)$$

where F_R denotes the heat removal factor, $(\tau\alpha)$ represents the effective transmittance-absorptance product, U_L is the overall heat loss coefficient, T_{fm} is the mean temperature of the fluid and T_a is the ambient temperature. It can also be calculated in terms of U_L and mean temperature of an absorber plate (T_{pm}):

$$Qu = A_c[I(\tau\alpha) - U_L(T_{pm} - T_a)]. \quad (10)$$

2.1.7. The collector heat removal factor is calculated as

$$F_R = \frac{mC_P}{A_c U_L}\left[1 - \exp\left(-\frac{U_L F' A_c}{mC_P}\right)\right]. \quad (11)$$

Here, F' is the collector efficiency factor which can be calculated as

$$F' = \frac{\frac{1}{U_L}}{W\left[\frac{1}{U_L}(D+(W-D)F)\right]+\frac{1}{C_b}+\frac{1}{\pi D h_f}}, \quad (12)$$

where: W − tube spacing, F − fin efficiency D − diameter of the tube, C_b − bond conductance. The fin efficiency can be calculated as [14]

$$F = \frac{\tanh\left(m\frac{W-D}{2}\right)}{m\frac{W-D}{2}}. \quad (13)$$

2.1.8. New mean temperature of the absorber plate is calculated as

$$T_{pm} = T_{in} + \frac{Qu}{A_c F_R U_L}(1 - F_R). \quad (14)$$

2.1.9. The collector's heat transfer coefficient can be calculated as

$$h_{nf} = \frac{\mathrm{Nu}k_{nf}}{D_{ir}}, \quad (15)$$

where Nu is the Nusselt number and D_{ir} is the tube's inner diameter.

2.1.10. The Reynolds number can be calculated as

$$\mathrm{Re}_{nf} = \frac{\rho_{nf} V D_{ir}}{\mu_{nf}}. \quad (16)$$

2.1.11. Prandtl number can be calculated as

$$\mathrm{Pr}_{nf} = \frac{\mu_{nf} C_{P,nf}}{k_{nf}}. \quad (17)$$

2.1.12. The average temperature of the flow can be calculated as

$$T_{avg} = T_{fm} = \frac{T_{out}+T_{in}}{2}. \quad (18)$$

2.1.13. The Nusselt number for a flat-plate collector having nanoparticles is evaluated using the correlation [24−27]:

$$\mathrm{Nu}_{np} = \frac{\frac{f}{8}(\mathrm{Re}-1000)\mathrm{Pr}}{1+12.7\left(\frac{f}{8}\right)^{\frac{1}{2}}\left(\mathrm{Pr}^{\frac{2}{3}}-1\right)}. \quad (19)$$

2.1.14. The Nusselt number for a water-based flat-plate collector is obtained from

$$\mathrm{Nu}_{bf} = 0.023\mathrm{Re}^{0.8}\mathrm{Pr}^{0.4}. \quad (20)$$

2.1.15. The friction factor is evaluated using the formula

$$f = [0.79\ln(\mathrm{Re}) - 1.64)]^{-2}. \quad (21)$$

Table 2. Thermophysical properties of various nanoparticles and water [21−26].

Nanoparticle Type	Formula	Density, (kg/m^3)	Specific heat, (J/kgK)	Thermal conductivity (W/m K)
Copper oxide	CuO	6000	551	34
Copper	Cu	8978	388	381
Alumina oxide	Al_2O_3	3960	774	40
Water	H_2O	997	4180	0.607

3. Results and discussion

3.1. Evaluation of thermophysical properties

The thermophysical properties of various nanoparticles and water are provided in Table 2. Figures 2 to 7 show the effect of different parameters on thermophysical properties of copper-based nanofluid flat-plate collector and their comparison with the properties of water-based collector.

Figure 2 shows the variation of nanofluid density (ρ_{nf}) with change in the nanoparticles volume fraction (ϕ) from 0.02 to 0.95 (3 values for the present analysis), which was evaluated using Eq. (1). It can be seen that the density of nanofluid is increasing with an increase in ϕ.

Figure 3 represents the effect of temperature rise parameter ($\Delta T/I$) on the nanofluid density, where $\Delta T = T_{fo} - T_{fi}$. For the present analysis, parameter ($\Delta T/I$) was taken in the range of 0.0018 to 0.026, whereas the value of solar radiation (I) is fixed at 900 W/m^2. Other system and operating parameters are given in detail in Table 1. It can be seen that the density of nanofluid with ϕ = 0.95 is the highest as compared to other ϕ values. But it can also be seen that water has a higher density than the nanofluid with ϕ = 0.02.

Figures 4 and 5 show the effect of volume fraction on the specific heat of nanofluid- and water-based collectors. It can be

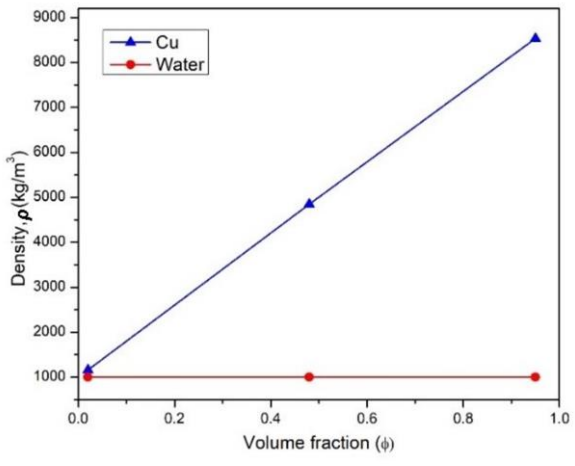

Fig. 2. Variation of density with volume fraction for copper-based nanofluids and water.

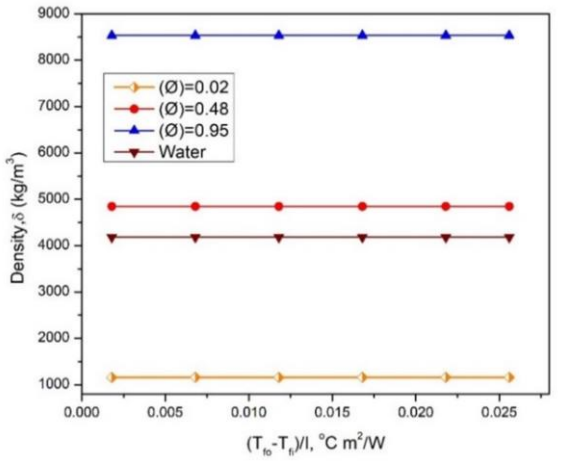

Fig. 3. Effect of temperature rise parameter on the density for copper-based nanofluids at different volume fractions and water.

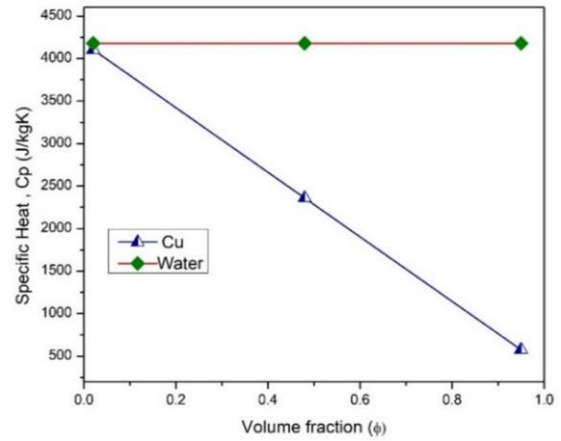

Fig. 4. Variation of specific heat with volume fraction for copper nanofluid and water-based collectors.

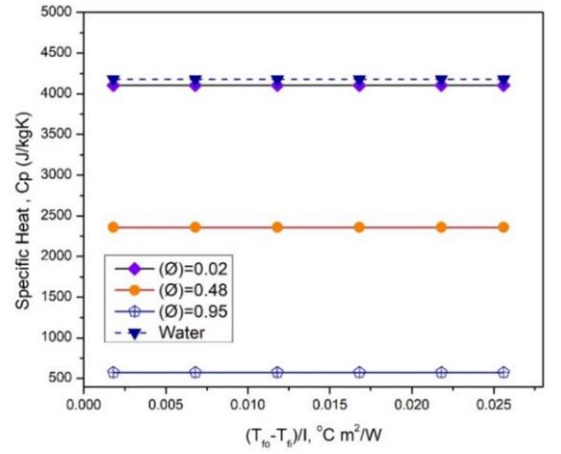

Fig. 5. Effect of temperature rise parameter on specific heat for copper nanofluid based collectors with different particle volume fractions and water based collector.

seen from Fig. 4 that the specific heat of nanofluid decreases with the increasing volume fraction of nanoparticles. From Fig. 5 it can be seen that specific heat shows inversely proportional values as ϕ increases. It can also be concluded from this figure that water have the highest specific heat compared to the considered nanofluids.

Figures 6 and 7 display thermal conductivity of a nanofluid as a function of volume fraction, and the comparison with the water thermal conductivity. It can be seen from Fig. 6 that the increase in thermal conductivity of the nanofluid is steeper when nanoparticle volume fractions exceeds 0.48. The thermal conductivity shows an enhancement which is directionally proportional to the increasing volume fraction of nanoparticles, owing to their better heat-conducting properties as compared to the base fluid. As the values of ϕ increase, more nanoparticles are added to the fluid, which enhances the thermal conductivity of nanofluid. Figure 7 demonstrates the variations of thermal conductivity with temperature rise parameter for different values of volume fraction. The thermal conductivity shows a similar trend as in Fig. 6.

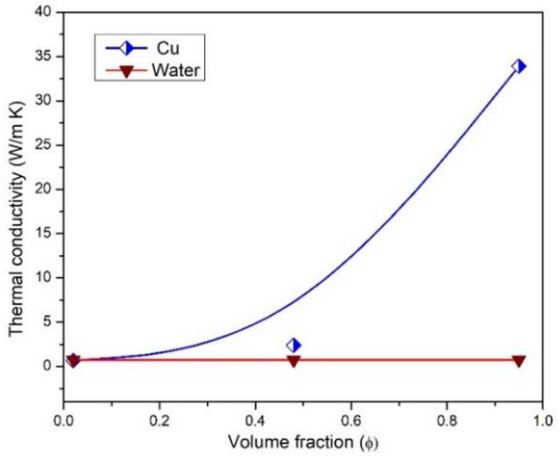

Fig. 6. Thermal conductivity of water and copper nanofluids with different volume fractions.

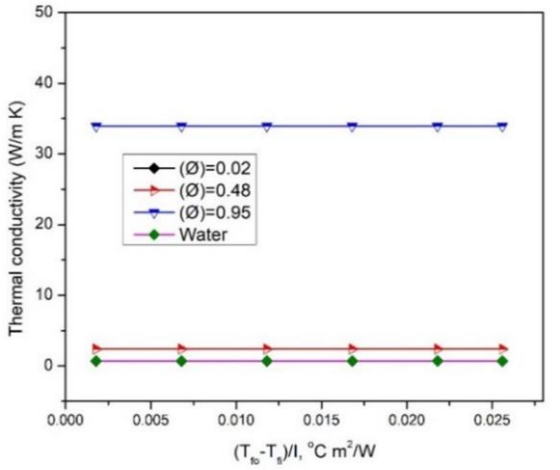

Fig. 7. Effect of temperature rise parameter for copper nanofluid collector with different particle volume fractions and water collector.

3.2. Evaluation of Reynolds number

Figure 8 presents the effect of the volume fraction on the Reynolds number (Re) of the nanofluid- and water-based collectors. The Reynolds number was evaluated using Eq. (16). It can be seen that while calculating Re, the density, velocity, and viscosity play the important role. It can be seen that the Reynolds number is decreased by increasing the volume fraction for the nanofluid-based collector while for the water collector it is constant. This is because when the volume fraction is increased, the nanofluid becomes more viscous, which makes the fluid more dense and more resistant to flow. This phenomenon reduces the fluid velocity, and as the Reynolds number depends on the fluid flow velocity, hence it results in lower values of Re. Moreover, as it can be seen from the figure, the highest value of mass flow rate corresponds with the highest value of the Reynolds number.

Figure 9 is presented to show the effect of the temperature rise parameter on the Reynolds number for different values of

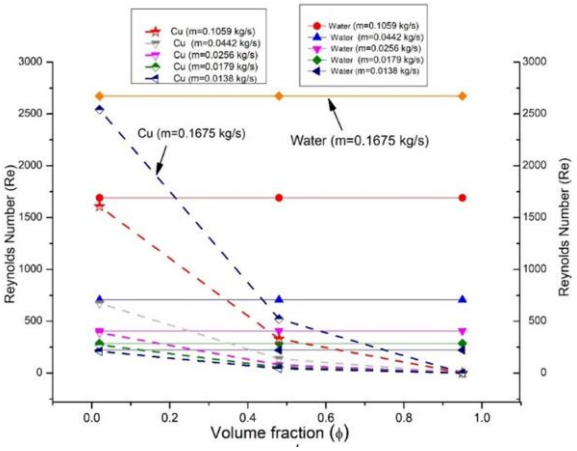

Fig. 8. Variation of Reynolds number with volume fraction for copper nanofluid and water for laminar and turbulent flow region.

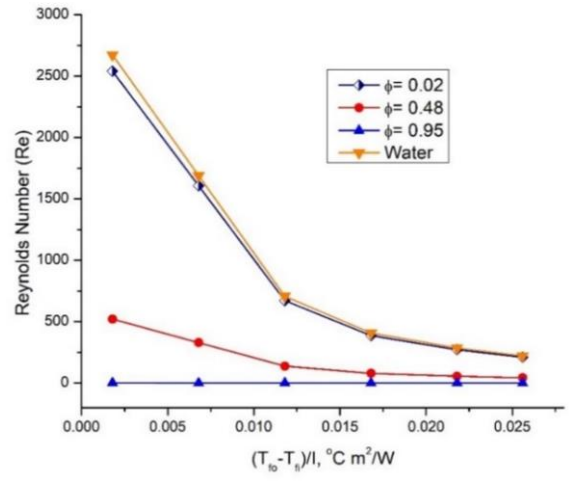

Fig. 9. Effect of temperature rise parameter on the Reynolds number for nanofluid-based and water solar collectors.

volume fraction. It can be seen from the figure that Re decreases with an increase in $\Delta T/I$. Among all curves, water collector has higher values of Re over the nanofluid-based collector for all values of $\Delta T/I$. Furthermore, the nanofluid-based collector with the lowest value of ϕ has higher values of Re over the collector using nanofluid with higher values of ϕ.

3.3. Evaluation of Nusselt number and heat transfer coefficient

Figure 10 shows the Nusselt number (Nu) variations with the change in volume fraction and for different values of mass flow rate (m), which has been evaluated using Eqs. (19) and (20) for nanofluid collector (Fig. 10a) and water-based collector (Fig. 10b), respectively. It can be seen that Nu of nanofluid collector decreases with an increase in ϕ. Adding more nanoparticles increases the nanofluid volume fraction, which increases the nanofluid viscosity and makes nanofluid thicker. Higher viscous fluids have less flowing ability and for the higher viscous fluid the rate of heat transfer is low, therefore the Nusselt number (Nu) decreases with an increase in the volume percentages of nanoparticles. Furthermore, it can also be concluded that the highest value of $\dot{m}$ shows the highest value of Nu for both types of collectors.

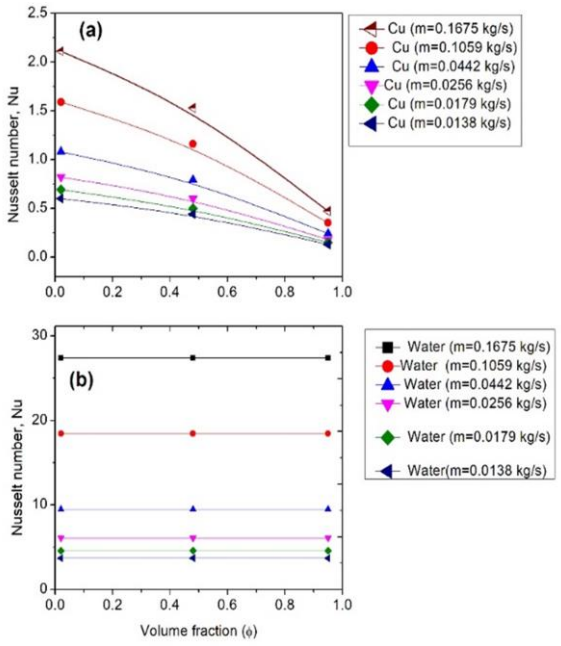

Fig. 10. Variation of Nusselt number with volume fraction for copper nanofluid (a) and water (b).

Figure 11 shows the variations of the Nusselt number with the temperature rise parameter for different volume fractions for both collectors. It can be seen that the Nu decreases with an increase in volume fraction (ϕ) from 0.02 to 0.95 for nanofluid collector. Furthermore, Nu values remain constant for all values of ϕ corresponding to increase in the values of ($\Delta T/I$). For water collector Nu decreases with an increase in the value of $\Delta T/I$ but the Nu values are higher as compared to nanofluid collector.

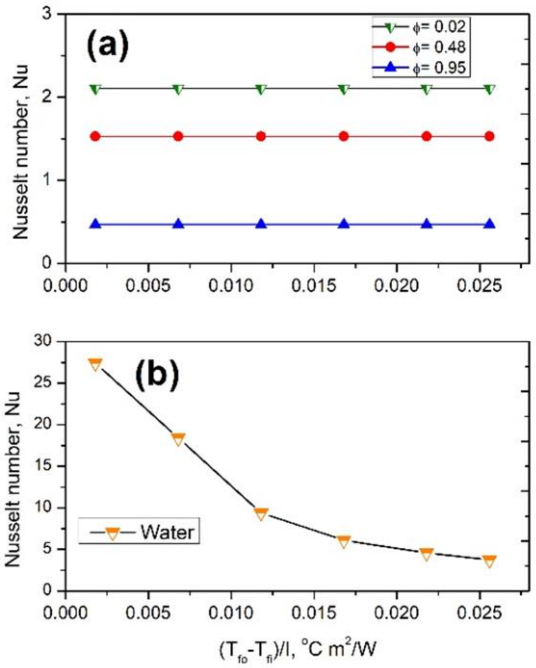

Fig. 11. Effect of temperature rise parameter on the Nusselt number for copper nanofluid at different volume fractions (a) and water (b).

3.4. Evaluation of heat transfer coefficient

Figure 12 shows the comparison of heat transfer coefficient (h) for nanofluid and water collectors for different values of volume fraction. It can be seen that for water collector (Fig. 12b), values

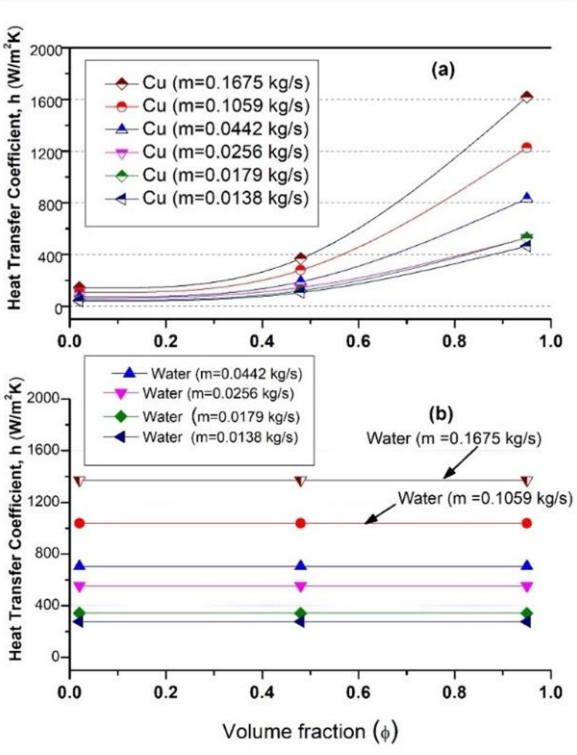

Fig. 12. Variation of heat transfer coefficient with volume fraction for copper nanofluid (a) and water (b).

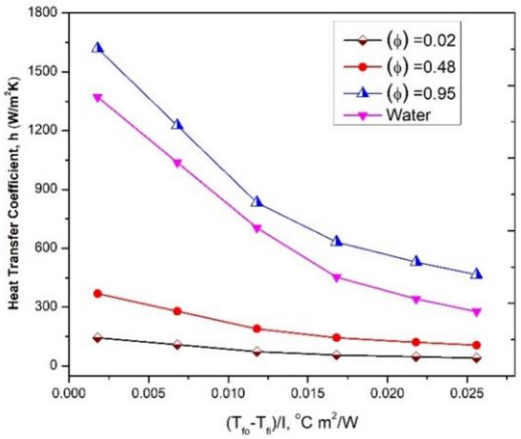

Fig. 13. Effect of temperature rise parameter on heat transfer coefficient for copper nanofluid collector with different particle volume fractions and water collector.

of h remain constant for all values of ϕ, but it is found that they increase with an increase in the values of m. While on the other side, it can be seen that for nanofluid collector (Fig. 12a) h is increasing with an increase in the value of ϕ and m.

Figure 13 shows the comparison of heat transfer coefficients of the nanofluid and water collectors for different values of temperature rise parameter and mass flow rate. It can be seen that for both collectors show decreasing values of h with an increase in the value of $\Delta T/I$. It can also be concluded from this figure that for nanofluid collector, the highest value of ϕ shows higher values of h over the other values of ϕ.

3.5. Evaluation of plate efficiency factor and heat removal factor

Figure 14 depicts a comparison of the collector plate efficiency factor (F_P) of the nanofluid-based and water-based collectors for different values of volume fraction and mass flow rate. As it can be seen, for both collectors F_P shows increasing values with an increase in m.

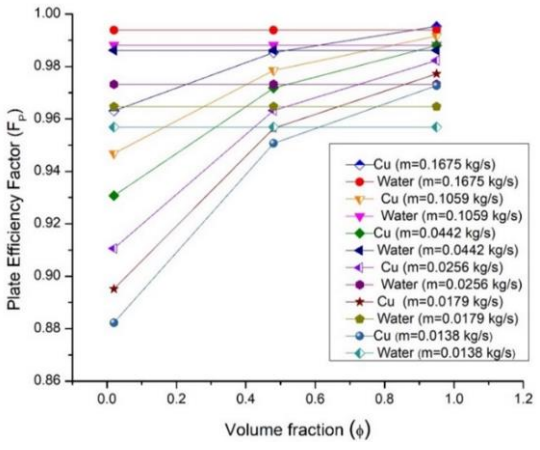

Fig. 14. Variation of plate efficiency factor with volume fraction for copper nanofluid and water collectors.

Figure 15 shows the effect of temperature rise parameter on the collector plate efficiency factor for nanofluid- and water-based collectors for different values of volume fraction. It can be seen that for both type of collectors F_P decreases with an increase in the value of $\Delta T/I$.

Figure 16 shows the collector heat removal factor (F_R) comparisons of nanofluid and water collectors for different values of volume fraction and mass flow rate. It can be seen from the figure that for nanofluid collector the value of F_R increases up to the values of ϕ = 0.45 and declines with further increase of ϕ.

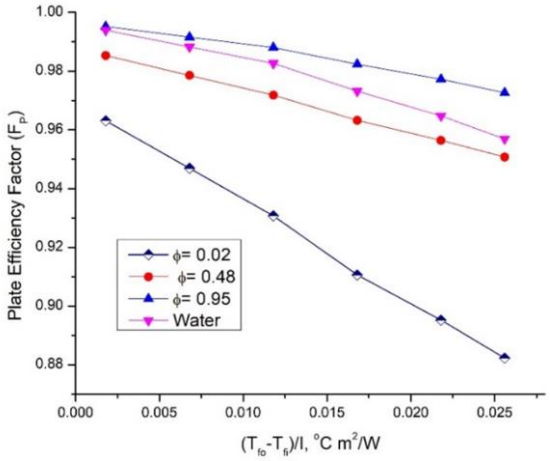

Fig. 15. Effect of temperature rise parameter on plate efficiency factor for copper nanofluid collector with different particle volume fractions and water collector.

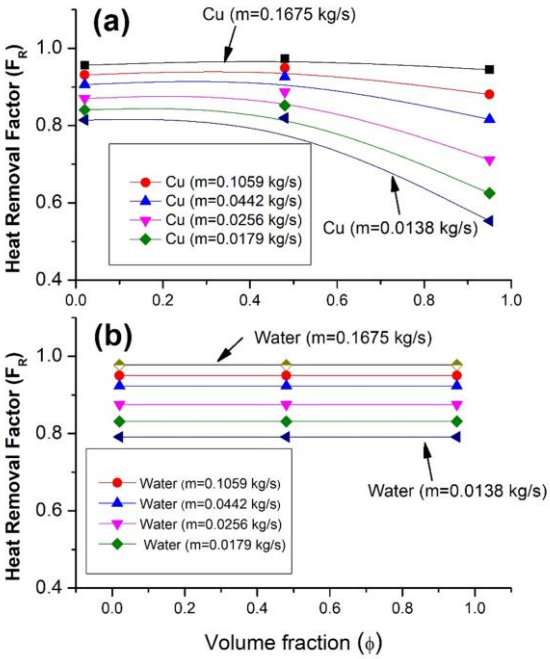

Fig. 16. Variation of heat removal factor with volume fraction for (a) copper nanofluid collector and (b) water collector.

Figure 17 shows a comparison of the heat removal factor of the nanofluid- and water-based collectors with changes in the

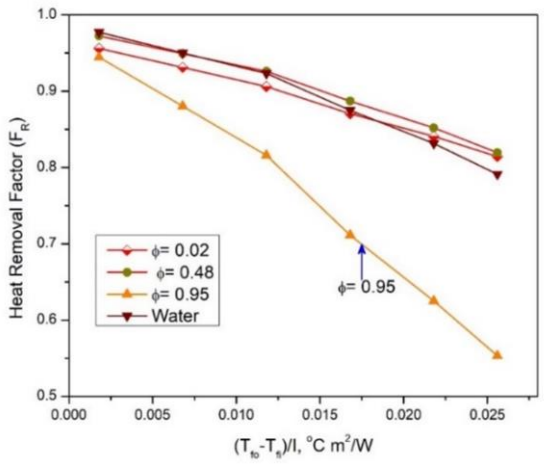

Fig. 17. Effect of temperature rise parameter on the plate efficiency factor for copper nanofluid collector with different particle volume fractions and water collector.

temperature rise parameter and volume fraction. For both collectors, it shows decreasing values of F_R with an increase in the value of $\Delta T/I$.

3.6. Evaluation of useful heat gain and energy efficiency

Figures 18−22 show variations of useful heat gain (Qu) and energy efficiency (η_{th}) of the nanofluid- and water-based collectors. It can be seen from these figures that nanofluid collector has higher values of Qu and η_{th} compared to water. This is because due to nanoparticles, nanofluid-based collector have higher thermal conductivity than water-based collector; these nanoparticles absorb more heat with the same collector surface area. In result, nanofluid collector has higher rate of heat exchange between the flowing fluid and collector surfaces (tubes).

Figure 18 shows a comparison of a collector useful heat gain between the nanofluid and water collectors for different values of volume fraction and mass flow rate. The results indicate that for water collector, Qu value increases with an increase in the values of m and it remain constant when ϕ increases, but for the nanofluid collector, it increases up to ϕ = 0.45. The Qu values for the nanofluid-based collector are higher compared to the water-based collector for all values of m and ϕ.

Figure 19 depicts a comparison of the useful heat gain variations with the temperature rise parameter between the water-based collector and nanofluid-based collectors with different nanoparticle volume fractions. For both collectors, Qu decreases with an increase in the values of $\Delta T/I$. It can also be seen from this figure that values of Qu for nanofluid collector are higher compared to the water based collector for all values of ϕ which used for the present nanofluid collector.

In Fig. 20 a comparison of a collector energy efficiency (η_{th}) between the nanofluid and water collectors as a function of volume fraction and mass flow rate. From the analysis it was found that water collector has attained maximum value of η_{th} = 53.7% for the highest value of m. Furthermore, the nanofluid collector

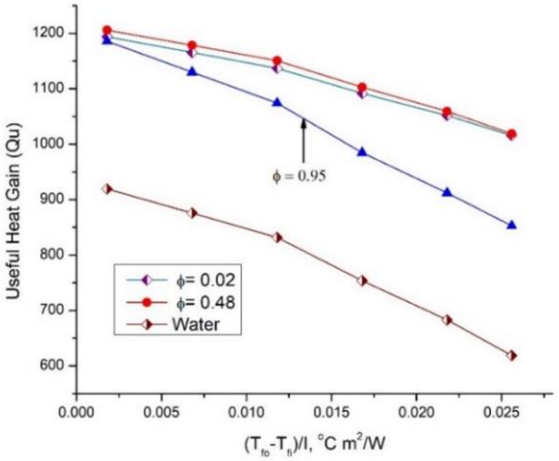

Fig. 19. Effect of temperature rise parameter on the useful heat gain for copper nanofluid collector with different particle volume fractions and water collector.

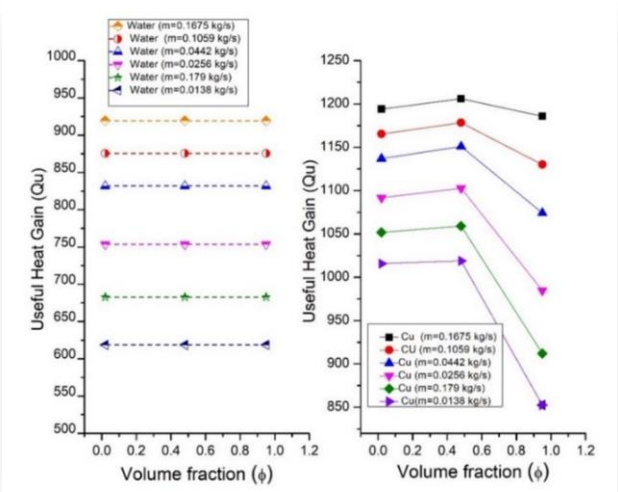

Fig. 18. Variation of useful heat gain with volume fraction for copper nanofluid and water-based collectors.

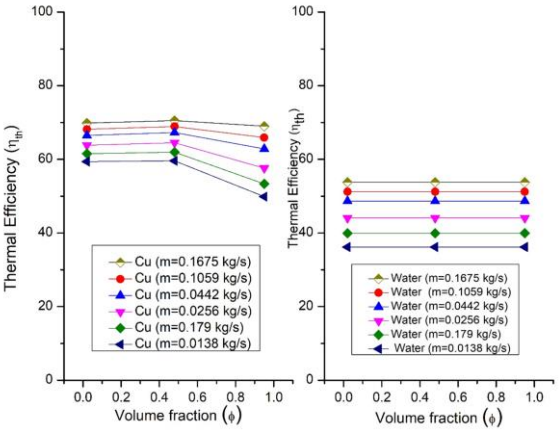

Fig. 20. Variation of energy efficiency with volume fraction for copper nanofluid and water-based collectors.

has maximum η_{th} of 70.5% for ϕ = 0.48 and the highest considered value of m. Thus the nanofluid collector was found to have 16.8% higher energy efficiency than the water collector.

Figure 21 presents the variation of collector energy efficiency (η_{th}) with the temperature rise parameter for the nanofluid-based collectors with different volume fractions of nanoparticles and the water based collector. It can be seen that for both types of collectors the value of η_{th} decrease with increasing values of $\Delta T/I$. It can also be found from the figure that water has values of η_{th} lower than those predicted for the nanofluid collector for all ϕ values considered.

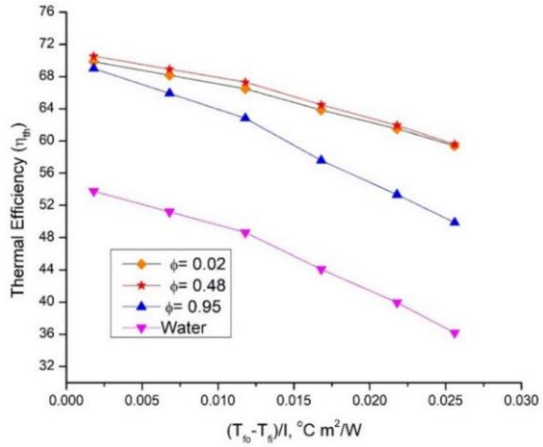

Fig. 21. Effect of temperature rise parameter on the collector energy efficiency for copper nanofluids with different particle volume fractions and water.

3.7. Evaluation of fluid outlet temperature

Figure 22 shows a comparison of the outlet fluid temperature (T_{fo}) between the nanofluid- and water-based collectors, changing with the volume fraction and for different values of mass flow rate. It can be seen that for both collector types T_{fo} decreases with an increase in m. From Fig. 22a it can be seen that for the water collector, T_{fo} is constant for all values of ϕ, i.e. no effect of ϕ is visible due to no presence of nanoparticles. Furthermore, from Fig. 22b it can be seen that T_{fo} for the nanofluid collector is increasing with enhancing the values of ϕ from 0.02 to 0.95. This is due to the fact that nanoparticles increase the surface area so that more solar energy is absorbed by the collector plate. Nanoparticles in the fluid also improve the convective heat transfer, which accelerates the heat absorption rate. So, finally the nanofluid based solar collector can extract more heat, which delivers the high fluid outlet temperature over the without nanoparticles based collector.

Figure 23 presents a comparison of the changes in the outlet fluid temperature with the temperature rise parameter between the nanofluid-based collectors at different volume fractions of nanoparticles and the water-based collector. It can be found that for both collector types, values of T_{fo} increase as the value of $\Delta T/I$ increase. It can also be seen from the figure that water collector exhibits lower T_{fo} values compared to the nanofluid collector for all considered ϕ values.

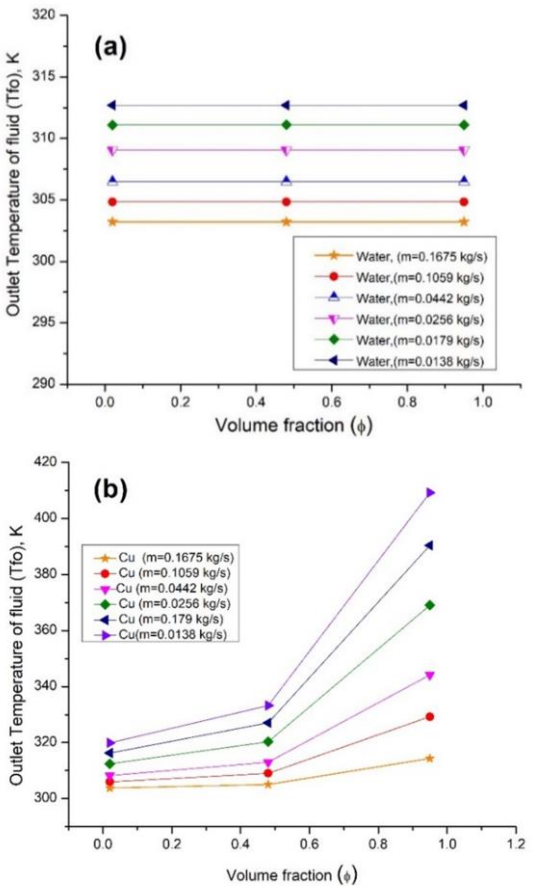

Fig. 22. Variation of the fluid outlet temperature with volume fraction for water (a) and copper nanofluid (b).

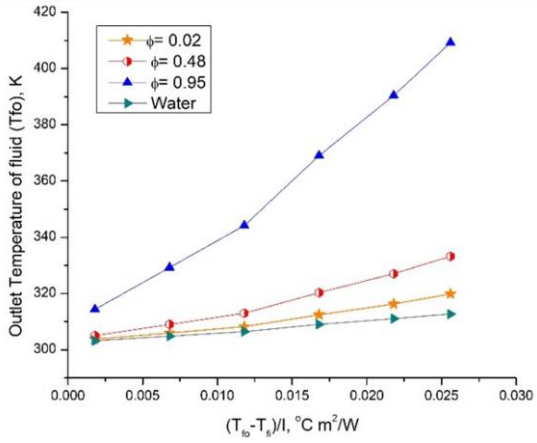

Fig. 23. Effect of the temperature rise parameter on fluid outlet temperature for water and for copper nanofluids with different particle volume fractions.

4. Optimal thermal and thermodynamic performance of collector

4.1. Evaluation of thermal efficiency improvement factor

In order to evaluate the enhancement of thermal performance of the thermal system after application of any technique and for comparison to the reference (base) system Sahu et al. [27] pro-

posed the parameter, called as thermal efficiency improvement factor (TEIF), which can be calculated as

$$\text{TEIF} = \frac{(\eta_{th})_{nf} - (\eta_{th})_{bf}}{(\eta_{th})_{bf}}. \quad (22)$$

Figure 24 shows the change of thermal efficiency improvement factor of a nanofluid collector with the volume fraction and for various values of mass flow rate. It can be seen from the figure that ϕ = 0.48 delivers the highest value of TEIF = 64.6% for the lowest value of *m*, while for the highest value of *m* the value of TEIF for ϕ = 0.48 is 31.1%.

Figure 25 demonstrates the variation of thermal efficiency improvement factor with the temperature rise parameter and volume fraction. It can be seen that ϕ = 0.48 shows the highest values of TEIF, while ϕ = 0.95 shows the lowest values of all ϕ considered for all values of $\Delta T/I$. Furthermore, TEIF values increase when the value of $\Delta T/I$ increases for all values of ϕ.

5.1. Evaluation of Sahu number

Figure 26 shows the effect of mass flow rate on the collector outlet fluid temperature (T_{fo}) for all values of volume fraction which were considered in the present analysis. It is clear from this figure that for both collector types, outlet temperature decreases with an increase in the mass flow rate. For mass flow rate exceeding 0.06 kg/s, T_{fo} decreases at a higher rate. At mass flow rates larger than *m* = 0.12 kg/s, for water collector and for the nanofluid collector of ϕ = 0.02 and 0.48, the values of T_{fo} are almost close to the collectors inlet temperature T_{fi} (shown by horizontal dotted line), i.e. both collector types show negligible temperature rise. Furthermore, it can also be concluded that as the mass flow rate increases, the outlet fluid temperature of the nanofluid collector is higher than that for the water collector. From the present analysis, it was found that the trends of changes in collector outlet fluid temperature and energy efficiency with mass flow rate are opposite.

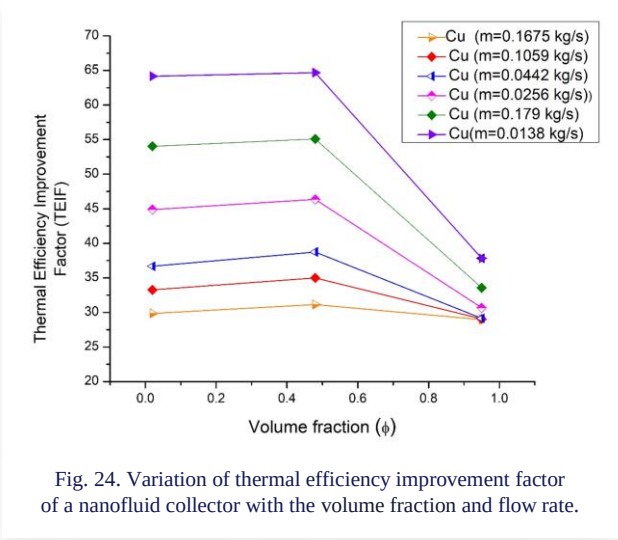

Fig. 24. Variation of thermal efficiency improvement factor of a nanofluid collector with the volume fraction and flow rate.

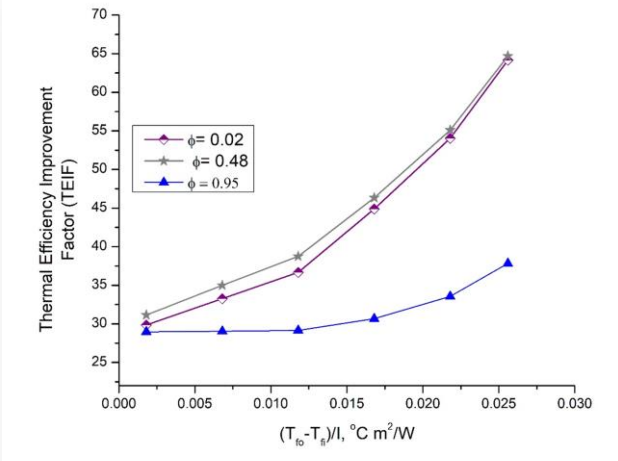

Fig. 25. Effect of temperature rise parameter on the thermal efficiency improvement factor for the present nanofluid collector.

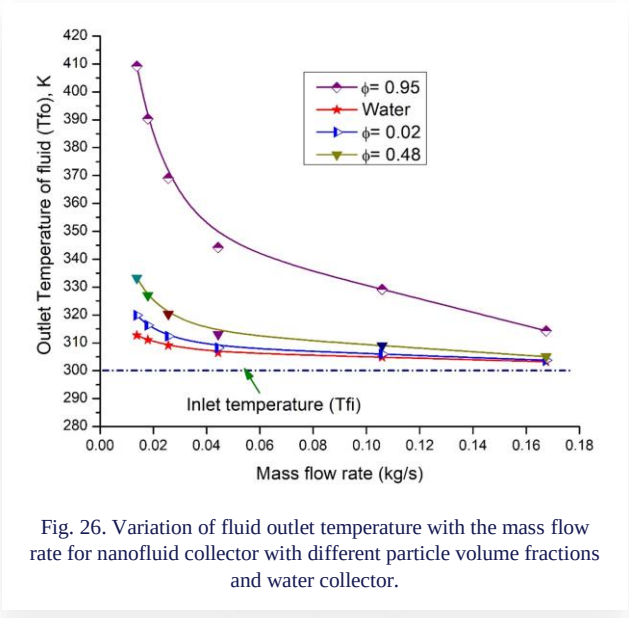

Fig. 26. Variation of fluid outlet temperature with the mass flow rate for nanofluid collector with different particle volume fractions and water collector.

It can be seen from Fig. 26 that collector outlet fluid temperature decreases with the increasing mass flow rate and at higher values of mass flow rate, the values of the collector outlet fluid temperature (T_{fo}) are very close to the inlet fluid temperature (T_{fi}). As per the authors' knowledge, any dimensionless number has been suggested to date by any investigator to evaluate the percentage of collector outlet fluid temperature with its operating mass flow rate. So, this manuscript fourth author suggested the following formula to evaluate this:

$$\text{Sahu Number} = 100 - \left(\frac{T_{fo}}{T_{fo} - T_{fi}}\right). \quad (23)$$

Figure 27 shows the variation of Sahu number with the mass flow rate for both collector types using Eq. (23). It can be seen from the figure that Sahu number is decreasing with *m* for both types of collectors. Furthermore, it can be concluded that for water and for nanofluid for all values of ϕ, after certain values of *m* Sahu number goes below zero (shown by vertical dotted lines for water and nanofluid solar collectors) to the negative values; this means after this value of m collectors are not able to deliver the temperature rise ($\Delta T = T_{fo} - T_{fi}$) significantly. For example, from Fig. 27 we can obtain the critical value of *m* = 0.07 kg/s for water by simply putting the vertical line towards the horizontal coordinate (flowrate–axis). Similarly, for nanofluid collector of

ϕ = 0.02 the critical value of m is 0.095 kg/s. Thus, it can be seen that the Sahu number is an effective number to obtain the optimal value of m for both types of collectors.

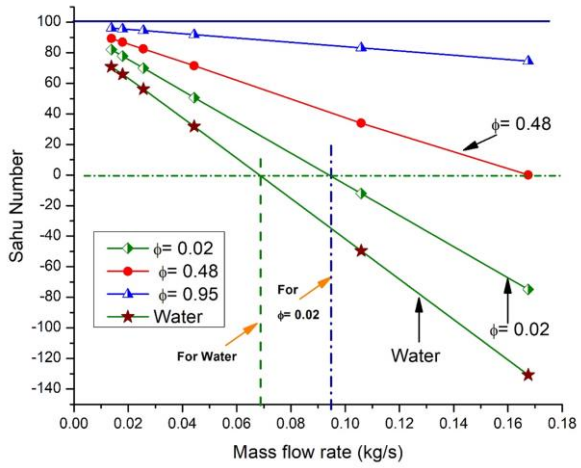

Fig. 27. Variation of Sahu number with the mass flow rate for nanofluid and water collectors.

6. Conclusions

In the present work the performances of the copper water-based flat plate solar collectors were examined theoretically using MATLAB. The effects of the temperature rise parameter, $\Delta T/I$ = 0.0018–0.025, volume fraction ϕ = 0–1 and mass flow rate, m = 0.012–0.170 kg/s, were considered in the investigation. Then a detailed parametric study was carried out to investigate the effects of volume fraction and mass flow rate, thermophysical properties, Nusselt number, heat transfer coefficient, collector plate factor, heat removal factor, Reynolds number, collector heat gain, fluid outlet temperature, and thermal efficiency. The Sahu number was introduced to find the optimum values of mass flow rate for both collector types. The main findings of the present work can be summarised as follows:

1. With increasing nanoparticles' volume fraction, the density and thermal conductivity of nanofluids based flat-plate collector improves, while the specific heat decreases.
2. With increasing volume fraction, the Reynolds number and Nusselt number of a nanofluid collector decreases.
3. With increasing volume fraction, the heat transfer coefficient, useful heat gain and collector fluid outlet temperature increase, but their values are higher compared to water (H_2O)-based collector for all values of volume fraction.
4. From the analysis it was found that the water collector has attained a maximum value of η_{th} = 53.7% for the highest value of mass flow rate. Furthermore, for the nanofluid collector, the maximum thermal efficiency is 70.5% for ϕ = 0.48 and for the highest value of mass flow rate, thus a maximum of 16.8% higher efficiency compared to a water collector was obtained.
5. The highest value of the thermal efficiency improvement factor equal to 64.6% was obtained for ϕ = 0.48 and for the lowest value of the mass flow rate, while for the highest value of mass flow rate, the value of thermal efficiency improvement factor for ϕ = 0.48 is 31.1%.
6. The Sahu number is an effective number to obtain the optimal value of mass flow rate for both types of collectors.

References

[1] Duffie, J.A., & Beckman, W.A. (2016). *Solar engineering of thermal processes solar engineering*, Wiley, New York. doi: 10.1002/9781118671603

[2] Kasaeian, A., Eshghi, A.T., & Sameti, M. (2015). A review on the applications of nanofluids in solar energy systems. *Renewable and Sustainable Energy Reviews*, 43, 584–598. doi: 10.1016/j.rser.2014.11.020

[3] Mahian, O., Kianifar, A., Kalogirou, S.A., Pop, I., & Wongwises, S. (2013). A review of the applications of nanofluids in solar energy. *International Journal of Heat and Mass Transfer*, 57(2), 582–594. doi: 10.1016/j.ijheatmasstransfer.2012.10.037

[4] Okonkwo, E.C., Osho, I.W., Almanassra, I.W., Abdullatif, Y.M., & Al-Ansari T. (2020). An updated review of nanofluids in various heat transfer devices. *Journal of Thermal Analysis and Calorimetry*, 145, 2817–2872. doi: 10.1007/s10973-020-09760-2

[5] Xian, H.W., Sidik, N.A.C., & Najafi, G. (2019). Recent state of nanofluid in automobile cooling systems. *Journal of Thermal Analysis and Calorimetry*, 135, 981–1008. doi: 10.1007/s10973-018-7477-3

[6] Sarsam, W.S., Kazi, S.N., & Badarudin, A. (2015). A review of studies on using nanofluids in flat-plate solar collectors. *Solar Energy*, 122, 1245–1265. doi: 10.1016/j.solener.2015.10.032

[7] Sajid, M.U., & Ali, H.M. (2019). Recent advances in application of nanofluids in heat transfer devices: A critical review. *Renewable and Sustainable Energy Reviews*, 103, 556–592. doi: 10.1016/j.rser.2018.12.057

[8] Choi, S.U.S, &. Eastman, J.A. (1995). Enhancing thermal conductivity of fluids with nanoparticles. *International Mechanical Engineering Congress and Exhibition*, 12-17 Nov., San Francisco, USA.

[9] Alim, M.A., Abdin, Z., Saidur, R., Hepbasli, A., Khairul, M.A., & Rahim, N.A. (2013). Analyses of entropy generation and pressure drop for a conventional flat plate solar collector using different types of metal oxide nanofluids. *Energy and Buildings*, 66, 289–96. doi: 10.1016/j.enbuild.2013.07.027

[10] Moghadam, A.J., Farzane-Gord, M., Sajadi, M., & Hoseyn-Zadeh, M. (2014). Effects of CuO/water nanofluid on the efficiency of a flat-plate solar collector. *Experimental Thermal and Fluid Science*, 58, 9–14. doi: 10.1016/j.expthermflusci.2014.06. 014

[11] Shojaeizadeh, E., Veysi, F., & Kamandi, A., (2015). Exergy efficiency investigation and optimization of an Al_2O_3-water nanofluid based flat-plate solar collector. *Energy and Buildings*, 101, 12–23. doi: 10.1016/j.enbuild.2015.04.04

[12] Mahian, O., Kianifar, A.,. Sahin, A.Z., & Wongwises, S. (2014). Entropy generation during Al2O3/water nanofluid flow in a solar collector: Effects of tube roughness, nanoparticle size, and different thermophysical models. *International Journal of Heat and Mass Transfer*, 78, 64–75. doi: 10.1016/j.ijheatmasstransfer.2014.06.051

[13] Said, Z., Saidur, R., Rahim, N.A., & Alim, M.A. (2014). Analyses of exergy efficiency and pumping power for a conventional flat plate solar collector using SWCNTs based nanofluid. *Energy and Buildings*, 78, 1–9. doi: 10.1016/j.enbuild.2014.03.061

[14] Sint, N.K.C., Choudhury, I.A., Masjuki, H.H., & Aoyama, H. (2017). Theoretical analysis to determine the efficiency of a CuO-water nanofluid based-flat plate solar collector for domestic solar

water heating system in Myanmar. *Solar Energy*, 155, 608–619. doi: 10.1016/j.solener.2017.06.055

[15] Tong, Y., Lee, H., Kang, W., & Cho, H., (2019). Energy and exergy comparison of a flat plate solar collector using water, Al_2O_3 nanofluid, and CuO nanofluid. *Applied Thermal* Engineering, 159, 113959. doi: 10.1016/j.applthermaleng.2019.113959

[16] Esen, H., Ozgen, F., Esen, M., & Sengur, A. (2009). Modelling of a new solar air heater through least-squares support vector machines. *Expert Systems with Applications*, 36(7), 10673–10682. doi: 10.1016/j.eswa.2009.02.045

[17] Esen, H., Ozgen, F., Esen, M., & Sengur, A. (2009). Artificial neural network and wavelet neural network approaches for modelling of a solar air heater. *Expert Systems with Applications*, 36(8), 11240–11248. doi: 10.1016/j.eswa.2009.02.073

[18] Ozgen, F., Esen, M., & Esen, H. (2009). Experimental investigation of thermal performance of a double-flow solar air heater having aluminium cans. *Renewable Energy*, 34(11), 2391–2398. doi 10.1016/j.renene.2009.03.029

[19] Esen, M., & Esen, H. (2005). Experimental investigation of a two-phase closed thermosyphon solar water heater. *Solar Energy*, 79(5), 459–468. doi: 10.1016/j.solener.2005.01.001

[20] Oflaz, F., Keklikcioglu, O., & Ozceyhan, V. (2022). Investigating thermal performance of combined use of SiO2-water nanofluid and newly designed conical wire inserts. *Case Studies in Thermal Engineering*, 38, 102378. doi: 10.1016/j.csite.2022.102378

[21] Wole-osho, I., Okonkwo, E.C., Abbasoglu, S., & Kavaz, D. (2020). Nanofluids in solar thermal collectors: Review and limitations. *International Journal of Thermophysics*, 41, 157. doi: 10.1007/s10765-020-02737-1

[22] Meibodi, S.S., Kianifar, A., Mahian, O., & Wongwises, S. (2016). Second law analysis of a nanofluid-based solar collector using experimental data. *Journal of Thermal Analysis and Calorimetry*, 126, 617–625. doi: 10.1007/s10973-016-5522-7

[23] He, Q., Zeng, S., & Wang, S. (2015). Experimental investigation on the efficiency of flat-plate solar collectors with nanofluids. *Applied Thermal Engineering*, 88, 165–171. doi: 10.1016/j.applthermaleng.2014.09.053

[24] Mahian, O., Kianifar, A., Sahin, A.Z., & Wongwises, S. (2015). Heat transfer, pressure drop, and entropy generation in a solar collector using SiO2/water nanofluids: Effects of nanoparticle size and pH. *Journal of Heat and Mass Transfer*, 137(6), 61011. doi: 10.1115/1.4029870

[25] Sarsam, W.S., Kazi, S.N., & Badarudin, A. (2015). A review of studies on using nanofluids in flat-plate solar collectors. *Solar Energy*, 122, 1245–1265. doi: 10.1016/j.solener.2015.10.032

[26] Khanafer, K., & Vafai, K. (2018). A review on the applications of nanofluids in solar energy field. *Renewable Energy*, 123, 398–406. doi: 10.1016/j.renene.2018.01.097

[27] Sahu, M.K., & Prasad, R.K. (2017). Thermohydraulic performance analysis of an arc shape wire roughened solar air heater. *Renewable Energy*, 108, 598–614. doi: 10.1016/j.renene.2017.02.075